ISSN 1063-7729, Astronomy Reports, 2008, Vol. 52, No. 9, pp. 714–728. © Pleiades Publishing, Ltd., 2008.
Original Russian Text © A.S. Gusev, V.I. Myakutin, A.E. Piskunov, F.K. Sakhibov, M.S. Khramtsova, 2008, published in Astronomicheskiĭ Zhurnal, 2008, Vol. 85, No. 9, pp. 794–809.

Age and Interstellar Absorption in Young Star-Formation Regions in the Galaxies NGC 1068, NGC 4449, NGC 4490, NGC 4631, and NGC 4656/57 Derived from Multicolor Photometry

A. S. Gusev[1], V. I. Myakutin[2], A. E. Piskunov[2], F. K. Sakhibov[3,4], and M. S. Khramtsova[5]

[1]*Sternberg Astronomical Institute, Universitetskiĭ pr. 13, Moscow, 119991, Russia*
[2]*Institute of Astronomy, Russian Academy of Sciences, ul. Pyatnitskaya 48, Moscow, 109017 Russia*
[3]*Giessen–Friedberg University for Applied Studies, Friedberg, Germany*
[4]*Institute of Astrophysics, Academy of Sciences of Tajikistan, ul. Bukhoro 22, Dushanbe, 734670 Tajikistan*
[5]*Ural State University, pr. Lenina 51, Yekaterinburg, 620083*

Received October 3, 2007; in final form, October, 26, 2007

Abstract—We have compared the results of multicolor $UBVR$ and Hα photometry for 169 young star-formation complexes in five galaxies using a grid of evolutionary models for young star clusters. The ages and interstellar absorptions are estimated for 102 star-formation complexes with the standard uncertainties $\sigma_t = 0.30$ dex and $\sigma_{A_V} = 0.45^m$. The accuracies of these parameters were verified using numerical simulations.

PACS numbers: 98.52.Nr, 98.62.Ai, 97.10.Bt
DOI: 10.1134/S1063772908090035

1. INTRODUCTION

The evolution of galaxies depends on their history of star formation, i.e., the history of variations of the star-formation rate, in many ways. The present chemical compositions of stellar populations, the gas and dust components, and the abundances of chemical elements depend in various ways on the history of star formation—the engine that transforms diffuse matter into stars. In contrast to the theory of stellar evolution, the theory of star formation has not reached the level necessary for applied studies, and the birth of stars is described using a parametrical approach. It is usually assumed that star formation can be adequately described by two functions—the initial mass function (IMF), which characterizes the mass distribution of newly forming stars, and the star-formation rate (SFR), which characterizes the intensity of this process. The main problem that has been faced in all studies of galactic evolution (and which still remains important) is interpretating the results of multicolor photometry and spectroscopy of star-formation regions in the nearest galaxies in terms of the IMF and SFR. In our previous studies, we called this the "inverse problem of star formation".

At the IAU General Assembly in 1994 [1], we suggested a then unique approach, whose essence is as follows. First, when interpreting observations, we should not restrict our consideration to one or several evolutionary models, instead considering a set of models encompassing the entire interval of the IMF and SFR. As the capabilities of calculations have increased, our model grid has become more and more detailed. It currently consists of 13 284 nodes, including 5508 models with an instantaneous star-formation mode (IB) and 7776 models with an extended mode (EB). The model grid is described in [2–5], together with the difference between our approach and classical methods for evolutionary and empirical population syntheses, along with a detailed list of references regarding the history of the method.

Our approach excludes from the physical parameters to be derived the interstellar absorption A_V and the chemical composition (or, more precisely, the abundance of heavy elements or metallicity, Z), which can be obtained independently from spectral observations. We thereby avoid the degeneracy of the age–absorption and age–chemical composition relationships described by Scalo [6]. The calculation of an intrinsic grid of evolutionary models for each studied object is required, consistent with the observed chemical composition, which strongly restricts the number of available objects with the required observational data. For this reason, we have not yet considered the multicolor photometry of about 200 young star-formation complexes (SFCs) in the galaxies NGC 1068, NGC 4051, NGC 4449,

NGC 4490, NGC 4631, and NGC 4656 obtained in the 1970s by I.I. Pronik and her colleagues, although these observations were processed by M.A. Smirnov, and their results are discussed in [7].

It was latershown using numerical experiments [2] that, even in the absence of an independent interstellar-absorption measurement A_V, a comparison of the reddened integrated colors of a cluster and the grid of evolutionary models can be used to estimate the interstellar absorption with an accuracy of $\sigma_{A_V} \approx 0.12^m$ and the age with an accuracy of 0.15 dex. Taking into account the observational errors in the color indices (0.05^m), the overall accuracies become $\sigma_{A_V} = 0.20^m$ and 0.22 dex. These experiments also showed that reliable derivation of the IMF in the absence of *a priori* absorption data is not possible. Note that these experiments were carried out for a fixed metallicity Z.

Indirect estimates for the interstellar absorption in the absence of spectral observations of SFCs are of particular interest. If it is also possible in this case to estimate the ages of SFCs with some accuracy, this can contribute substantially to studies of the star-formation history in galaxies. Therefore, our prime objective here is to interpret the results of multicolor photometry of about 169 SFCs in the galaxies NGC 1068, NGC 4449, NGC 4490, NGC 4631, and NGC 4656. NGC 4051 was excluded from consideration due to the low accuracy of its measured color indices $B-V$ (in the photometric system of the Crimean Observatory-2 [7]).

Since we consider here SFCs for which only multicolor photometry is available, while the spectra remain unknown, we have studied separately the possibility of estimating the interstellar absorptions and ages (and their accuracy) based on these data. The possibility of estimating the IMF is ruled out in advance, as follows from the results of the numerical experiments [2].

Section 2 briefly describes the used set (or space) of evolutionary models. Supplementary numerical experiments carried out to estimate the uncertainties of the unknown parameters (the age t, interstellar absorption A_V, and heavy-element abundance Z) are presented in Section 3. Section 4 contains the results of multicolor photometry of SFCs in the studied galaxies. In Section 5, we compare the multicolor photometry of these SFCs with the grid of evolutionary models and determine the ages and extinctions in the studied SFCs. Our results are discussed in Section 6.

2. THE INASAN GRID OF EVOLUTIONARY MODELS AND THE REAL COLORS OF YOUNG SFCS

We use here the INASAN models [8], which encompass a wide interval of IMF parameters and ages and two elementary limiting modes of star formation, with an instantaneous star-formation burst (IB) and ongoing, extended star-formation bursts (EB). The evolutionary tracks for the models were calculated for ages 10^6-10^9 years. The upper limit for the IMF mass ranged from 5 to $120M_\odot$, while the IMF slope α ranged from $\alpha = -5.35$ (a very steep IMF) to $\alpha = -0.35$ (a relatively flat IMF). The slope $\alpha = -2.35$ corresponds to the well-known Salpeter IMF [9].

The nature of the objects studied here—SFCs and giant HII regions with sizes of 100 to 300 pc—enables us to restrict the intervals of variation for the age and the upper limit of the IMF mass. As was already discussed in [3], with a gas velocity of 15–30 km/s, the lifetime of an HII region with a size of 100 pc is 3–7 million years. The size of the studied SFCs often reach 200–300 pc. The lifetimes of such giant HII regions can reach 20 million years, and they can exist longer only if there is some gas reservoir along which a wave of star formation propagates; i.e., if the EB mode occurs. Therefore, regions with the IB star-formation mode will be observed as HII regions with ages up to some maximum corresponding to a single region of ionized hydrogen. Older SFCs with the IB mode cannot contain giant regions of ionized hydrogen. Therefore, we restricted the grid of evolutionary models for the IB mode to a age of 20 million years. The grid of models for the EB mode was restricted to an age of 100 million years. The adopted age restrictions overestimate the age interval for the studied giant HII regions.

To form a giant HII region, a large flux of ionizing radiation is needed, which can be provided only by massive O stars ($M > 15M_\odot$). Therefore, the upper mass limit for our grid is restricted to the interval $M_{max} \in (30, 120)M_\odot$.

In two-color diagrams, this set of evolutionary models covers the relatively narrow color intervals [2, 8]

$$U-B \in (-1.22, -0.17),$$
$$B-V \in (-0.33, 0.08),$$
$$V-R \in (-0.20, 0.35).$$

Therefore, objects that obviously (given the measurement errors) lie beyond these limits are sure to be susceptible to the effects of interstellar absorption.

In [2], we formulated a criterion for estimating the interstellar absorption using a grid of evolutionary models, according to which the colors corrected for A_V should correspond as closely as possible to those for some model (a grid node). This node was found by searching for the deepest minimum of a deviation functional calculated for the given grid. By deviation functional, we have in mind a numerical function that assigns to each node some number

characterizing the deviation of the observed photometric values from the model values. The means used to calculate the functional can be found in [2–5]. A brief description of the evolutionary models is also presented in [2, 5], while the models themselves are discussed in detail in [8].

Recall only that the theoretical color indices are calculated as functions of α, M_{max}, t, Z, and the star-formation mode.

Here, we are particularly interested in the impact of variations of Z on the accuracy of the derived ages. We showed earlier in [8] that, in the presence of variations of Z within $Z > 0.5Z_\odot$, the effect of metallicity on the$(U-B)-(B-V)$ two-color diagram is insignificant compared to the impact of variations of the age and IMF slope.

3. DERIVING THE OF PHYSICAL CHARACTERISTICS OF SFCS WITH UNKNOWN INTERSTELLAR ABSORPTIONS AND METALLICITY. NUMERICAL SIMULATIONS

We carried out numerical simulations to investigate of how precisely the interstellar absorption, and possibly the age, of a stellar population can be determined when the metallicity is unknown. The procedure used for these simulations is described in detail in [2], where we assumed that the metallicity Z was known from independent spectral measurements. Therefore, the grid of evolutionary tracks with which the trial star-cluster models were compared was calculated in advance for a specified Z.

The main distinction of the simulations carried out in our study is that the metallicity of the trial model is taken to be unknown. Therefore, the model colors are compared with tracks calculated for 10 different metallicities from $Z = 0.004$ to $Z = 0.040$ with a step of $h_Z = 0.004$. Thus, we have added another dimension to the multi-dimension grid of evolutionary tracks, increasing the number of nodes to 132 840 (i.e., by a factor of 10 compared to our previous simulations).

As was shown in [8], the evolutionary models are only weakly sensitive to variations of Z; therefore, the selected initial step $h_Z = 0.004$ seems sufficient to follow the variations of the integrated colors with variations in Z.

Our simulations indicate the average accuracy of our model metallicity estimates to be $\Delta Z = \pm 0.010$ (Fig. 1). Since the metallicity of the trial models was taken to be equal to the solar value $Z_\odot$, the scatter $\Delta Z = \pm 0.010$ means that the estimates for the heavy-element abundance basically lie in the interval $Z/Z_\odot \in (0.5, 1.6)$.

It was shown in [8] that the colors for evolutionary tracks for $Z > 0.5Z_\odot$ differ by values comparable to the accuracy of the color measurements. In the EB mode, the evolutionary tracks with low metallicity, $Z < 0.5Z_\odot$, also differ little from the tracks with $Z > 0.5Z_\odot$.

According to the numerical simulations described in [2], given the weak sensitivity of the models to variations of Z, a high accuracy in the interstellar absorption A_V is expected. Recall that the colors of the trial models were "corrupted" by both random measurement errors and the randomly specified interstellar absorption $A_V(input)$, as is described in [2].

The aim of the simulations was to find an $A_V(output)$ that is ideally equal to $A_V(input)$; i.e., to reconstruct the true colors of our trial model with accuracy up to the random measurement errors. Figure 1b presents the relationship between input absorption $A_V(input)$ and the absorption $A_V(output)$ obtained at the end of the simulations. This is a linear relation with a high correlation coefficient ($r = 0.98$). The standard error in the interstellar absorption is $\sigma_{A_V} = 0.22^m$, which is close to the standard accuracy $\sigma_{A_V} = 0.20^m$ obtained in [2] for similar random color errors, with Z known beforehand.

The age estimates t_{output} are correlated with the ages of the trial models t_{input} somewhat more poorly than the absorption: $r = 0.8$ (Fig. 2a). The standard error in the ages, $\sigma_t = 0.30$ dex on a logarithmic scale, reflects the errors in both the metallicity estimates and the IMF slope α. With unknown Z, the IMF slope can be determined only poorly, and its estimates for real objects cannot be considered reliable (Fig. 2b).

4. MULTICOLOR PHOTOMETRY OF SFCS IN NGC 1068, NGC 4449, NGC 4490, NGC 4631, AND NGC 4656/57

Our multicolor photometry of young star-formation regions (giant HII regions) was carried out in eight spectral bands centered on emission lines, as well as in spectral intervals without emission lines (the stellar continuum). The measurements were carried out by M.A. Smirnov from frames obtained in 1966–1981 by I.I. Pronik and her colleagues at the Crimean Astrophysical Observatory (Ukraine) using the 2.6-m Shain Telescope with an electro-optical transducer (EOT). The color system and measurement procedure were identical to those used in previous studies of multicolor photometry of galaxies and their constituents [12–20]. From two to six frames were obtained in each spectral interval for each galaxy.

The measurements were transformed to absolute fluxes in energy units using extrafocal images of

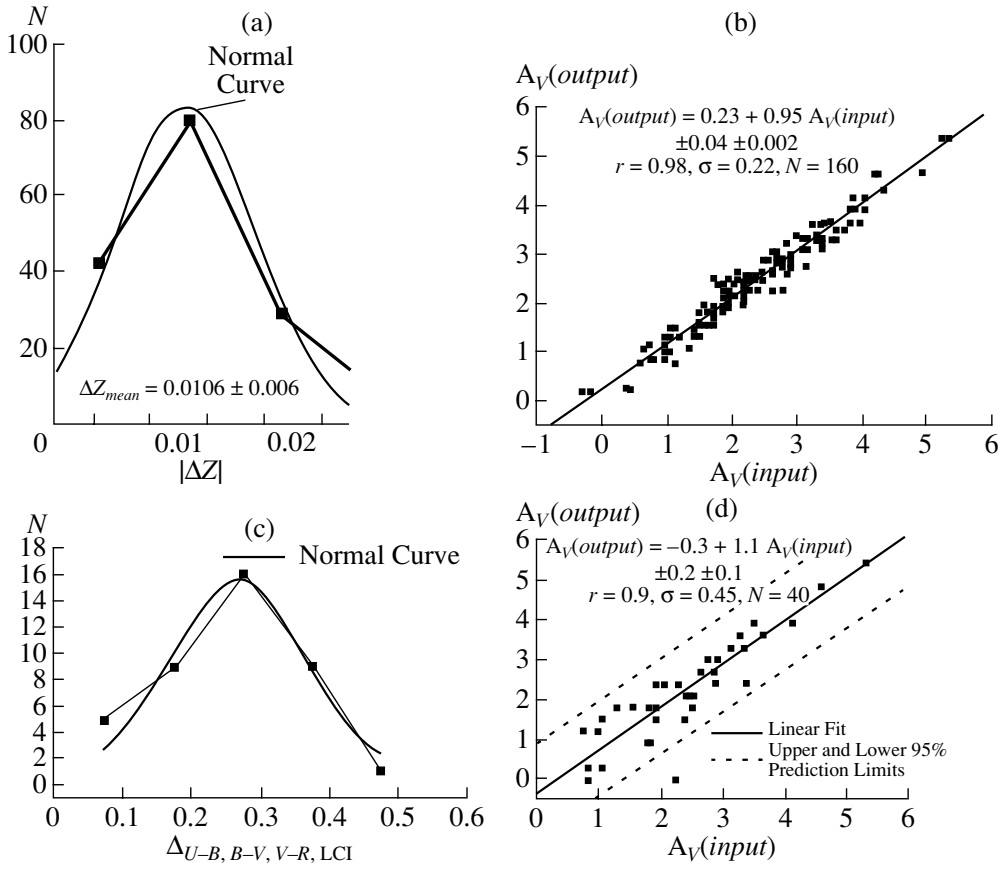

Fig. 1. Results of numerical simulations with the grid of models for the metallicity and interstellar absorption: (a) distribution of the errors in Z for 160 cluster models (the average uncertainty is $\Delta Z = \pm 0.010$); (b) relation between the initial and final absorptions ($A_V(input)$ and $A_V(output)$) obtained taking into account the internal formal uncertainty in the color measurements ($\sim 0.05^m$); (c) distribution of the total random error corresponding to the external uncertainty in the color measurements introduced into the model colors in the numerical simulations; (d) relation between the initial and final absorptions ($A_V(input)$ and $A_V(output)$) obtained taking into account the external uncertainty in the color measurements ($\sim 0.10^m - 0.20^m$).

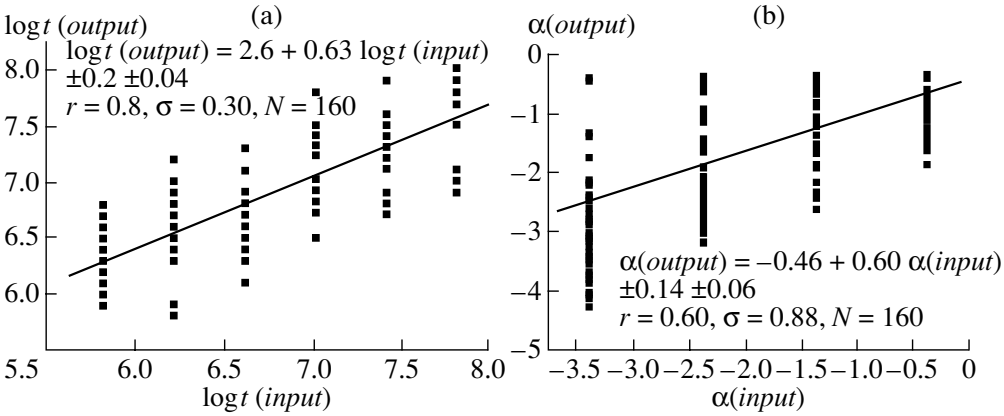

Fig. 2. Results of the numerical simulations in the model grid for the ages and IMF slopes: (a) derived age – initial age relation for the trial model; (b) derived IMF slope – initial IMF slope relation for the trial model.

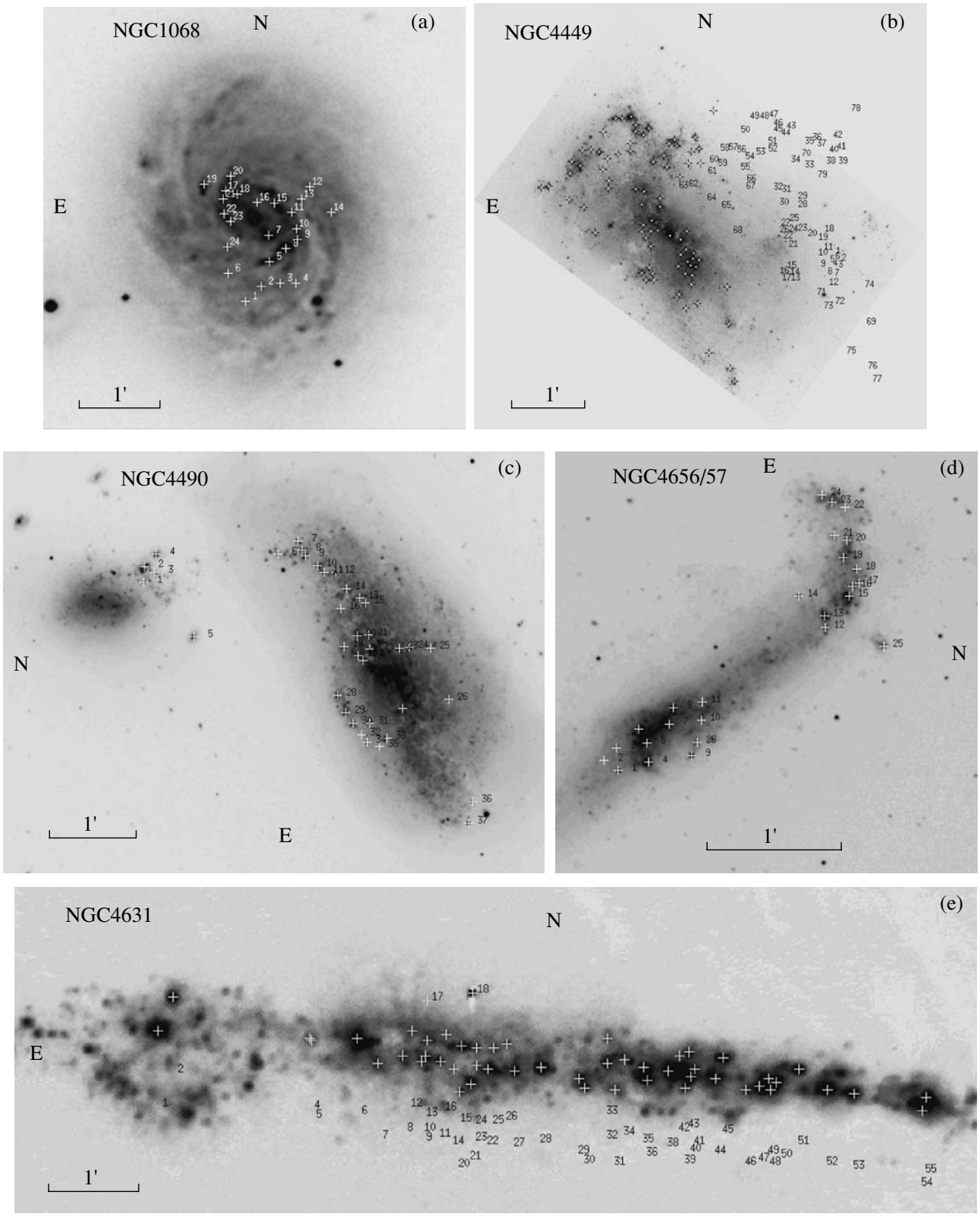

Fig. 3. Identification maps for the objects in (a) NGC 1068, (b) NGC 4449, (c) NGC 4490, (d) NGC 4631, and (e) NGC 4656/57.

the stars 76 Coma and 49 Pleiades obtained on the same dates. The non-uniform background of the galaxy was taken into account using measurements in the immediate vicinity of the SFCs. We reduced the measurements [7] to the Johnson [21] $UBVR\mathrm{H}\alpha$ photometric system. Figure 3 presents identification maps for the SFCs in NGC 1068, NGC 4449, NGC 4490, NGC 4631, NGC 4656/57. Table 1 (which can be found in electronic form at http://lnfm1.sai.msu.ru/~gusev/crao_tab1.dat) presents the $U-B$, $B-V$, $V-R$, and LCI values obtained by M.A. Smirnov for 169 SFCs in the five galaxies (see below for the definition of the LCI parameter). Table 1 does not contain all the objects marked in the images of the galaxies (Fig. 3).

In the course of measuring the frames obtained in the Crimean photometric system, we found systematic errors in the zero-point calibration for the transformation of darkenings (photographic densities) to intensity [7] in a number of cases. This results in substantial errors in the SFC colors, noted in various studies of the Crimean photometric system [17]. Since the zero points are different for different series (groups) of observations, observations belonging to a single series (group) must be used in all spectral bands to determine the SFC colors. The existence of three zero points is due to the use of three different photometric curves to transform the measured darkenings of the photographic films into intensities, which was, in turn, due to the use of three photometric scales imprinted into each frame. It was not always possible to take into account the systematic error in the zero point for the darkening to intensity transformation. Therefore, although the intrinsic color measurements are available for all the objects marked in the galaxy frames, not all these objects are included in Table 1.

To describe the radiation in the Lyman continuum, a supplementary color was introduced—the Lyman continuum index $\mathrm{LCI} = 2 - \log\left(\frac{F_{\mathrm{H}\alpha+[\mathrm{NII}]}}{F_B}\right)$, where $F_{\mathrm{H}\alpha+[\mathrm{NII}]}$ is the flux in close hydrogen and nitrogen emission lines and F_B the flux in the stellar continuum in the B band. Column 7 of Table 1 contains the B brightness and column 8 the size of the diaphragm, which corresponded to the sizes of the images of the objects in the $\mathrm{H}\alpha + [\mathrm{NII}]$ filter (in arcseconds). The absence of the expected correlation between the brightnesses and sizes of the objects (columns 7 and 8) may indicate that the values in column 8 do not correspond to the true sizes of the SFCs.

Our analysis in [7] (comparisons with the results of other authors) showed that the uncertainties in the Crimean color measurements based on EOT photometry are $\sigma_{U-B} = 0.13^m$, $\sigma_{B-V} = 0.19^m$, $\sigma_{V-R} < 0.15^m$, and $\sigma_{\mathrm{LCI}} = 0.10^m$. Here, we mean the external accuracy of these color measurements, which we estimated via pairwise comparisons with color measurements carried out by various authors using different techniques.

It was shown in [5, 7] that the uncertainty of photographic measurements of SFC colors (both direct and obtained with an EOT) is essentially the same as that of more accurate CCD observations. This can apparently be explained by the fact that the main sources of errors in SFC photometry are uncertainties in discriminating the object against the galactic background, correcting for this background radiation, and determining the SFC's size, rather than errors in the observed brightness of the object. In this respect, photographic and electro-optical measurements of SFCs in the considered studies differ little. The formal internal accuracies presented in studies based on CCD observations are substantially higher, approximately 0.05^m. The formal or internal errors of photographic observations (using EOTs) of the studied galaxies is also significantly higher (0.05^m–0.08^m). However, due to the above reasons, the external accuracy of the color observations for all techniques remains lower by a factor of two to three. We carried out numerical simulations to determine the interstellar absorption when the level of the random errors corresponds to the external accuracy of the color indices, 0.10^m–0.20^m. In this case, the expected uncertainty in the absorption is $\sigma_{A_V} = 0.45^m$ (Figs. 1c,d). The corresponding uncertainty in the color excesses, $\sim 0.14^m$, is comparable to the observational accuracy of the color excesses obtained from the Balmer decrement for the same SFCs in NGC 4631 [22].

5. COMPARISON OF THE SFC MULTICOLOR PHOTOMETRY AND THE INASAN GRID OF EVOLUTIONARY MODELS

Figure 4 compares the observed SFC colors with the INASAN grid [8] in the two-color diagram. As we can see (Fig. 4a), the observed SFC color indices are "redder" than those assumed by the theoretical models: the objects are systematically shifted to the right and upwards in the diagram. Since the diagram presents a grid for fixed metallicity and an upper limit for the stellar mass ($Z = Z_\odot, M_{max} = 90M_\odot$), the variations of these values extend beyond the region occupied by the evolutionary models. In Fig. 4a, this region is restricted by the solid lines.

In [8], we showed that the spectral energy distributions of evolutionary models are only weakly sensitive to variations of Z. In Section 3, we studied the accuracy of the derived interstellar absorption values using the deviation functionals for unknown Z.

The numerical simulations have shown that with the external accuracies of the color indices are

Table 1. Photometry of SFCs in galaxies

NGC	№	$U-B$	$B-V$	$V-R$	LCI	m_B	D, arcseconds	A_V	$\log t$ (years)	Δ
1	2	3	4	5	6	7	8	9	10	11
1068	1	−0.93	0.09	0.50	−0.11	17.23	6.0			
	2	−0.76	0.11	0.42	0.31	18.77	4.0	0.30	7.50	0.14
	3	−0.94	0.02	0.39	−0.03	18.84	5.0	0.00	7.50	0.22
	4	−0.80	0.09	0.40	0.09	17.82	5.0	0.15	7.50	0.14
	5	−0.53	0.36	0.04	−0.40	16.48	6.0	2.25	5.80	0.07
	6	−0.36	0.24	0.29	0.15	16.9	5.0	1.05	7.60	0.02
	7	−0.04	0.42	0.21	−0.08	16.86	5.0	1.80	7.10	0.04
	8	−0.70	0.34	0.55	−0.18	18.48	3.0	0.82	7.50	0.26
	9	−0.28	0.48	0.23	−0.09	17.89	5.0	2.40	6.40	0.00
	10	−0.68	0.28	0.21	−0.11	18.46	3.0	1.28	6.70	0.09
	11	0.00	0.37	0.63	−0.11	18.26	4.0	1.65	7.90	0.21
	12	−0.36	0.34	0.21	0.02	18.80	3.0	1.58	6.60	0.01
	13	−0.65	0.20	0.54	−0.27	19.63	4.0	0.60	7.60	0.19
	14	−0.62	0.16	0.11	−0.31	19.86	3.0	1.28	6.60	0.01
	15	−0.72	0.01	0.01	−0.12	16.55	6.0	0.52	6.60	0.01
	16	−0.04	0.36	0.20	−0.17	19.63	3.0	1.57	7.30	0.04
	17	−0.49	0.17	0.02	0.18	17.44	4.0	0.90	6.70	0.08
	18	−0.04	0.57	0.59	−0.26	19.71	3.0	1.87	8.00	0.06
	19	−0.21	0.40	0.61	−0.57	20.13	3.0	1.43	7.90	0.12
	20	−0.86	0.09	0.19	−0.21	20.39	2.5	0.67	6.70	0.12
	21	−0.57	0.57	0.51	−0.06	19.74	3.5	1.50	7.50	0.27
	22	−0.37	0.36	0.56	−0.07	17.73	6.0	1.20	7.70	0.09
	23	−0.40	0.19	0.55	−0.16	18.88	6.0	0.75	7.90	0.15
	24	−0.76	0.11	0.08	−0.09	19.30	4.0	0.97	6.60	0.03
4449	1	−0.85	0.10	0.24	0.02	15.10	4.0	0.23	7.50	0.13
	2	−1.14	−0.15	−0.05	−0.26	16.10	4.0	0.45	5.90	0.11
	3	−1.01	−0.20	0.32	−0.15	15.00	4.0	0.00	7.40	0.27
	4	−1.08	−0.12	−0.02	−0.27	15.00	4.0	0.60	5.90	0.10
	6	−0.92	0.01	0.05	−0.11	15.45	3.0	0.60	6.60	0.08
	7	−0.36	0.36		−0.29	17.54	2.5			
	8	−1.13	0.09		−0.29	17.40	2.5			
	9	−0.54	0.33		−0.20	17.03	2.5			
	10	−0.76	0.33		−0.42	16.87	2.5			
	11	−0.77	0.19		−0.30	16.71	4.0			
	12	−0.46	0.10		−0.28	17.80	2.5			

Table 1. (Contd.)

NGC	№	$U-B$	$B-V$	$V-R$	LCI	m_B	D, arcseconds	A_V	$\log t$ (years)	Δ
1	2	3	4	5	6	7	8	9	10	11
	13	−0.61				19.47	2.5			
	14	−0.53				19.35	4.0			
	15	−0.53	0.28	0.55	−0.12	16.7	7.1	0.90	7.60	0.14
	16	−0.52				18.43	3.0			
	17	−0.36				17.58	3.5			
	18	−0.76	−0.07	0.41	0.00	16.42	3.5	0.00	7.60	0.13
	19	−0.99	0.22	0.49	0.19	16.33	3.5			
	20	−0.52	0.18	0.35	0.53	14.	9.5	0.60	8.00	0.01
	21	−0.38	0.26	0.53	0.02	15.9	10.3	0.90	7.90	0.10
	22	−0.72	0.29		−0.30	17.12	3.0			
	23	−0.80	0.05		−0.06	16.32	3.0			
	24	−0.96	0.15	0.54	−0.76	15.05	6.0			
	25	−0.51	−0.07	0.40	0.51	16.1	7.1	0.00	8.00	0.15
	26	−0.34	0.35		0.26	16.23	4.0			
	27	−0.66	−0.02	0.40	0.11	15.6	8.2	0.00	7.80	0.09
	28		0.03	0.35	0.55	15.3	7.6			
	29	−0.78	0.04	0.52	−0.10	17.08	4.0	0.15	7.70	0.22
	30	−0.86	0.21	0.58	0.27	15.73	6.0			
	31	−0.90	0.04	0.16	0.54	15.6	10.0	0.52	6.70	0.11
	32		0.12	0.22	0.54	16.3	8.2			
	33	−0.36	0.16		−0.07	18.08	4.0			
	34	−0.84	0.19		0.03	16.51	5.0			
	35	−0.80	0.22		0.06	16.94	4.0			
	36		0.06	0.52	−0.04	16.8	8.1			
	37	−1.02	−0.24		−0.22	17.80	3.0			
	39	−1.02				19.91	2.0			
	40	−0.99				18.9	4.9			
	41	−0.90				17.88	4.0			
	42	−0.98	−0.18		−0.13	16.37	4.5			
	43		0.01	0.17	−0.13	17.3	4.5			
	44	−1.02	0.07		−0.02	12.10	35.0			
	45		0.23	0.50	0.20	16.4	4.5			
	46	−0.32	0.35	0.22	0.12	17.00	3.0	1.80	6.90	0.01
	47			0.18	−0.30	15.7	7.0			
	48	−0.98	0.06	0.27	−0.36	17.17	3.0	0.00	7.50	0.21

Table 1. (Contd.)

NGC	№	$U-B$	$B-V$	$V-R$	LCI	m_B	D, arcseconds	A_V	$\log t$ (years)	Δ
1	2	3	4	5	6	7	8	9	10	11
	49			0.16	−0.55	17.2	4.5			
	50	−0.92	−0.18		−0.26	18.55	3.0			
	51	−1.06	0.07		−0.07	18.78	2.0			
	52	−0.83	0.14		−0.06	17.31	5.0			
	53	−0.51				20.04	3.0			
	54	−0.92				19.91	2.0			
	56	−1.11	0.04	0.66	−0.47	16.9	5.9			
	57	−0.86				18.34	2.5			
	58	−0.88				20.26	2.5			
	59	−0.74	0.26	0.51	−0.22	15.6	12.0	0.60	7.50	0.23
	60	−0.64	0.19		−0.29	17.04	4.0			
	61	−0.70	0.32	0.51	−0.18	16.0	11.0	0.75	7.50	0.23
	62	−0.95	0.08		−0.52	20.04	2.5			
	63	−0.57	0.00		−0.25	17.80	4.5			
	64	−0.60				19.51	2.0			
	65	−0.72				18.08	4.0			
	66	−0.70				18.82	3.0			
	67	−1.02				19.35	2.0			
	68	−0.74	0.06		−0.12	17.23	5.0			
	69		−0.16	0.22	−0.22	17.2	7.0			
	70		0.12	0.32	0.60	15.00	20.0			
	71	−0.94	−0.03			19.64	2.5			
	72	−0.44	0.01			17.89	3.0			
	73	−0.86	0.05			18.27	3.0			
	74		−0.26			17.6	5.9			
	76	−0.90	0.47		0.05	18.94	4.0			
	77	−0.98	0.05		−0.04	17.93	5.0			
	78	−0.42	0.29		−0.42	18.00	3.0			
	79	−1.06	−0.20		0.09	18.50	3.0			
4490	2	−0.56	0.24	0.42	−0.51	17.60	7.6	0.75	7.50	0.05
	4	−0.70	0.06	0.19	−0.85	18.59	6.0	0.45	7.10	0.00
	5	−0.20	0.25	0.08	0.03	20.13	5.4	1.20	7.10	0.10
	6	−0.74	−0.20	0.18		19.52	3.8	0.00	7.20	0.09
	7	−0.82	−0.26	0.28	−0.76	19.56	4.4	0.00	7.50	0.20
	8	−0.68	−0.01	0.17	−0.69	19.32	3.9	0.08	7.60	0.01

Table 1. (Contd.)

NGC	№	$U-B$	$B-V$	$V-R$	LCI	m_B	D, arcseconds	A_V	$\log t$ (years)	Δ
1	2	3	4	5	6	7	8	9	10	11
	9	−1.10	−0.23	0.04	−0.67	18.57	5.9	0.00	6.60	0.11
	10	−0.62	−0.05	0.40	−1.22	18.14	8.9	0.00	7.90	0.10
	11	−0.88	−0.11	0.08	−0.69	19.46	3.8	0.08	6.90	0.01
	12	−0.52	0.07	0.42	−0.76	18.93	4.9	0.30	8.00	0.08
	13	−0.70	0.34	0.44	−0.35	18.06	5.7	0.75	7.50	0.21
	14	−0.89	−0.07	0.48	0.52	17.73	7.4	0.00	7.50	0.24
	15	−0.84	0.06	0.07	−0.55	18.99	6.3	0.75	6.60	0.06
	16	−0.22	0.53	0.58	−0.47	18.93	5.4	1.72	7.70	0.05
	17	−0.70	0.08	0.46	0.05	17.14	3.2	0.23	7.70	0.13
	18	−0.46	0.21	0.29	−0.24	15.56	10.1	0.60	7.10	0.01
	19	−0.92	−0.14	0.37	−0.86	17.61	6.0	0.00	7.50	0.21
	20	−0.22	0.30	0.27	−1.61	19.21	7.0	1.43	7.20	0.01
	21	−0.74	0.34	0.10	−0.87	18.34	4.0	1.95	5.80	0.12
	22	−0.34	0.35	0.37	−0.55	19.44	12.8	1.05	7.80	0.01
	23	−0.42	0.22	0.31	−0.79	17.98	6.4	0.75	7.70	0.01
	24	−0.68	0.18	0.28	−0.40	16.51	6.7	0.60	7.50	0.07
	25	−0.83	0.11	0.20	−0.73	17.95	7.3	0.75	6.70	0.11
	26	−0.92	−0.10	0.00	−0.60	19.57	4.8	0.38	6.60	0.01
	31	−0.37	0.36	0.30	−0.77	20.84	7.2	1.58	7.10	0.01
	32	−0.63	0.35	0.58	−0.30	16.30	1.3	0.97	7.50	0.23
4631	1	−0.36	0.06	0.38	−0.58	18.14	8.4	0.38	8.00	0.10
	6	−0.63	−0.01	0.15	−0.38	14.58	17.9	0.23	7.10	0.01
	7	−0.94	−0.15	0.17	0.14	17.01	11.6	0.00	6.80	0.09
	8	−0.60	0.13	0.33	−0.14	19.21	4.2	0.45	7.70	0.01
	9	−0.09	0.40	0.33	−0.27	19.13	4.6	1.58	7.60	0.01
	10	−0.44	0.13	0.06	−0.40	20.10	4.8	1.05	6.70	0.05
	11	−0.95	−0.17	0.04	−0.41	18.56	6.9	0.08	6.90	0.01
	12	−1.05	−0.21	0.11	−0.39	16.77	12.6	0.00	6.70	0.12
	13	−0.57	−0.18	−0.14	−0.32	16.43	13.6	0.00	7.10	0.15
	14	−0.27	0.27	0.68	−0.16	18.52	6.3	1.27	7.90	0.24
	15	−0.79	−0.08	0.28	−0.38	16.70	11.6	0.00	7.50	0.06
	16	−0.82	0.19	0.18	−0.16	16.91	10.5	0.90	6.70	0.14
	21	−0.92	0.03	0.17	−0.14	18.46	5.3	0.45	6.70	0.12
	22	−0.12	0.50	0.79	−0.43	18.06	8.4			
	24	−0.31	0.23	0.52	−0.10	19.47	3.2	0.90	8.00	0.12

Table 1. (Contd.)

NGC	№	$U-B$	$B-V$	$V-R$	LCI	m_B	D, arcseconds	A_V	$\log t$ (years)	Δ
1	2	3	4	5	6	7	8	9	10	11
	27	−0.50	0.37	0.12	−0.22	19.56	3.6	2.10	6.40	0.01
	28	−0.39	0.44	0.44	−0.17	17.05	8.4	1.50	7.50	0.04
	29	−0.36	0.26	0.51	−0.21	19.44	5.7	0.90	7.90	0.09
	30	−0.65	0.09	0.38	−0.29	17.77	6.9	0.30	7.60	0.04
	32	−1.19	0.00	0.01	−0.16	18.53	6.3	0.67	5.80	0.24
	33	−1.15	−0.07	0.11	−0.25	19.00	5.3	0.00	6.70	0.21
	34	−0.45	0.38	0.07	−0.28	20.10	3.6	1.80	6.50	0.08
	35	−0.41	0.49	0.26	−0.25	16.60	8.4	2.25	6.60	0.04
	36	−0.58	0.10	0.48	−0.38	16.79	9.4	0.45	7.70	0.11
	38	−0.88	−0.03	0.01	−0.58	17.34	9.4	0.90	5.90	0.03
	39	−0.88	0.04	0.31	−0.20	20.02	4.6	0.00	7.50	0.15
	40	−0.33	0.39	0.60	−0.57	18.76	6.9	1.35	7.70	0.12
	41	−0.47	0.33	0.28	−0.13	20.39	4.2	1.35	7.10	0.01
	44	−0.55	0.36	−0.01	−0.28	17.83	7.3	2.17	5.80	0.11
	45	−0.27	0.30	0.31	−0.36	19.47	5.3	1.20	7.60	0.01
	46	−0.97	0.06	0.39	−0.44	20.72	3.2	0.00	7.50	0.26
	47	−0.88	0.14	0.44	−0.32	18.12	7.3	0.15	7.50	0.24
	48	−0.54	0.36	0.48	−0.19	19.67	3.2	1.05	7.50	0.12
	49	−0.69	0.37	0.45	−0.18	18.21	5.3	0.82	7.50	0.23
	52	−0.76	0.00	0.04	−0.48	17.38	7.6	0.67	6.70	0.01
	53	−1.21	−0.11	0.21	−0.50	20.97	3.6			
4656/57	4	−0.44	−0.07	0.66	−0.23	15.8	7.3			
	5	−0.56	0.40	0.33	−0.31	17.38	6.3	1.42	6.80	0.12
	6	−0.38	0.20	0.16	−0.28	18.10	6.0	1.28	7.00	0.01
	7	−1.04	0.07	0.26	−0.06	17.40	6.0	0.15	6.80	0.27
	8	−0.34	0.24	0.38	0.27	17.80	6.0	0.75	8.00	0.01
	9	−0.54	0.19	0.55	−0.18	19.05	3.0	0.67	7.70	0.15
	10	−0.34	0.27	0.62	−0.27	17.60	7.0	1.05	7.90	0.17
	15	−0.74	0.19	0.24	−0.13	16.5	7.0	0.82	6.80	0.10
	26	−1.06	−0.03	0.00	−0.11	18.36	5.0	0.82	5.80	0.13

$\sigma_{U-B} = 0.13^m$, $\sigma_{B-V} = 0.19^m$, $\sigma_{V-R} < 0.15^m$, and $\sigma_{\rm LCI} = 0.10^m$, while the accuracy of the interstellar absorption is $\sigma_{A_V} = 0.45^m$ (Fig. 1c,d).

Since calculation of the deviation functional requires at least three different color indices, the number of objects for which the method is applicable decreases from 169 to 102. Figure 4b presents the positions of 102 SFCs relative to the theoretical models, after correctomg their observed colors for the interstellar absorption, A_V.

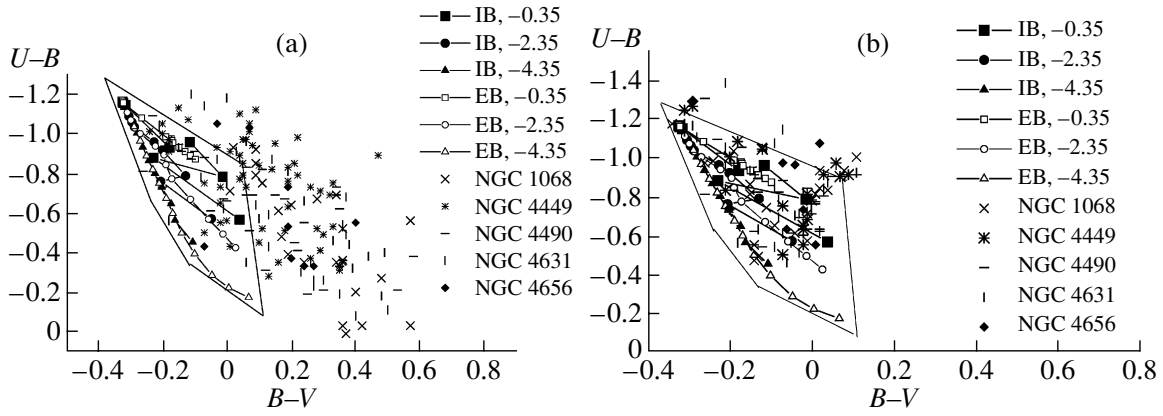

Fig. 4. Comparison of the SFC positions and the grid of evolutionary models in the two-color diagram: (a) SFC colors not corrected for A_V; (b) SFC colors corrected for A_V.

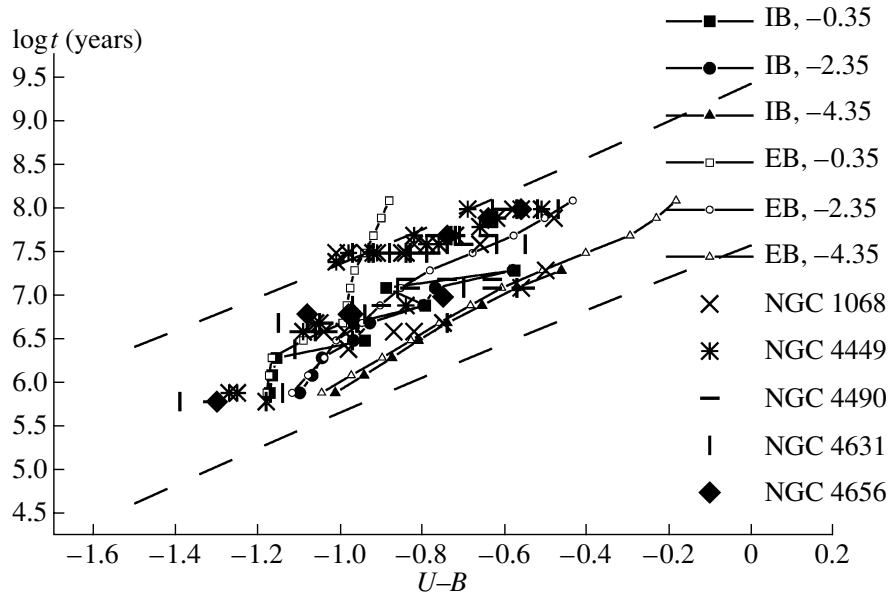

Fig. 5. Comparison between the positions of the SFCs and the evolutionary model grid in the age t–color $U-B$ diagram. The dashed lines restrict the interval of predicted theoretical ages at the 95% confidence level.

The interstellar absorptions for the studied SFCs are presented in column 9 of Table 1. Column 11 of Table 1 contains the "errors" in the colors corrected for the interstellar absorption, where the "errors" of the colors refer to the deviations of the color indices corrected for interstellar absorption from the theoretical colors for the nearest node of the evolutionary model grid.

Column 10 of Table 1 presents age estimates for the complexes. The position of the obtained age estimates in the t–$(U-B)$ diagram (Fig. 5) shows, for example, that the SFCs in NGC 1068 are inclined towards models with a steeper IMF slope than the SFCs in NGC 4449.

The age estimates for the real SFCs in the five studied galaxies lie within the 95% confidence interval of the linear regression model (the region restricted by the dashed lines)

$$\log t = (8.5 \pm 0.2) + (2.0 \pm 0.2) \times (U-B), \quad (1)$$

which describes the evolutionary model grid in Fig. 5 with a correlation of 76% and a standard error of $\sigma_{\log t} = 0.41$. The linear regression model describing the age distribution for 102 real SFCs with colors that

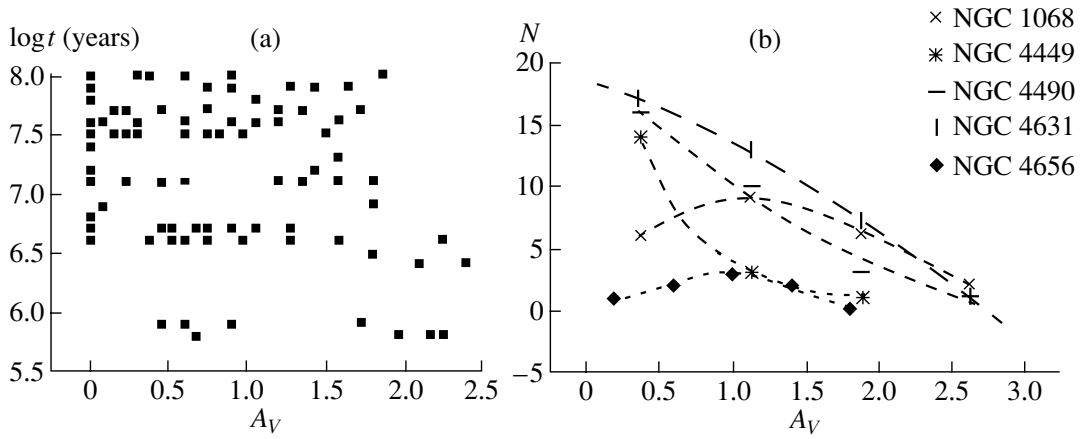

Fig. 6. (a) Age – interstellar absorption diagram, showing the absence of a correlation between these quantities. (b) Interstellar absorption distribution for five SFC samples in the studied galaxies.

differ little from the model (1) is

$$\log t = (9.1 \pm 0.2) + (2.3 \pm 0.2) \times (U-B) \quad (2)$$

with a correlation of 80% and a standard error of $\sigma_{\log t} = 0.37$.

6. RESULTS

To conclude, we will present our estimates of the ages and interstellar absorptions for 102 young SFCs in the studied galaxies.

The numerical simulations of [2] showed that the derivation of age and interstellar absorptions based on multicolor photometry using the deviation functional is not sensitive to age–absorption degeneracy. Let us verify the impact of this effect using our estimated ages and interstellar absorptions. Figure 6a clearly shows the absence of any correlation between these values.

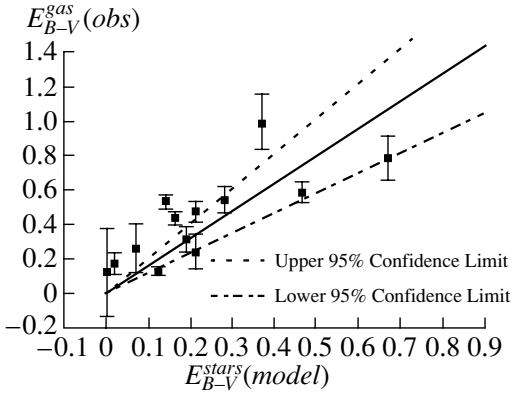

Fig. 7. Comparison of the obtained "stellar" color excesses $E^{stars}_{B-V}(model)$ and those derived from the Balmer decrement $E^{gas}_{B-V}(obs)$ for the SFCs in NGC 4631.

Figure 6b presents the distributions of our estimated interstellar absorptions for the SFC samples in the five studied galaxies. The distributions of A_V for the SFCs in NGC 1068 and NGC 4656 correspond to normal laws with the means $\overline{A_V} = 1.1^m \pm 0.6^m$ and $\overline{A_V} = 0.9^m \pm 0.4^m$, respectively. In NGC 4449 and NGC 4490, the number of SFC decreases exponentially with increasing A_V. In NGC 4631, the decrease in the number of SFCs with increasing A_V is described by a second-order polynomial. The parameters of the distributions are presented in Table 2. The interstellar absorption in an SFC reflects the distribution of interstellar dust [23], which may depend on the intensity of the interstellar wind in the SFC, which, in turn, depends on the number of high-mass stars, i.e., the IMF. It is possible that the differences in the interstellar-absorption distributions in the SFCs indirectly reflect the distributions of the IMF parameters in the studied galaxies. On the other hand, the absence of observational spectral estimates for the interstellar absorption and chemical composition hindered estimation of the IMF parameters in the studied SFCs. Therefore, observational estimates for the interstellar absorptions of the entire SFC sample within a galaxy are not only important for determinating the IMF in each complex, but also provide information about the distribution of interstellar matter and the activity of high-mass stars.

Figure 7 compares our "model" estimates for the color excess E^{stars}_{B-V} and the color excesses E^{gas}_{B-V} calculated from the observed Balmer decrement in NGC 4631 [22]. Since the criteria for discriminating an individual star formation region used in [22] were different from those used by M.A. Smirnov, this identification should be considered tentative.

In total, the objects discriminated in [22] are often larger, and include several of our objects. This made

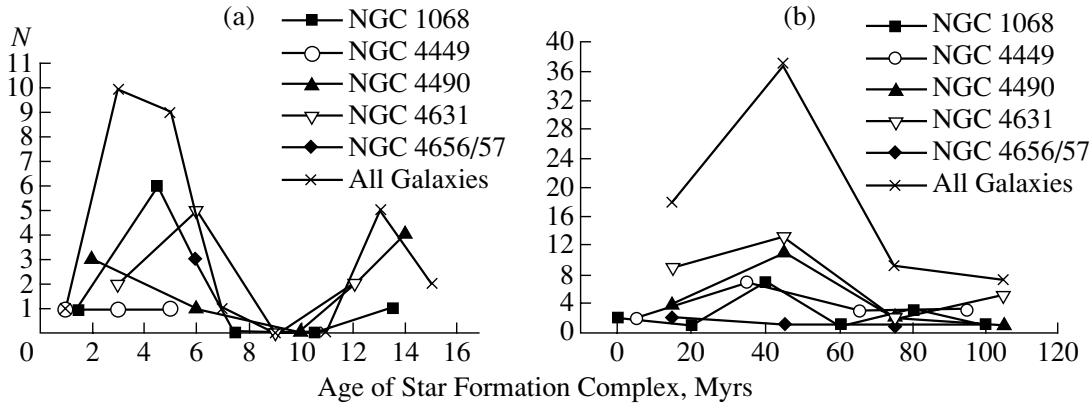

Fig. 8. Age distribution of SFCs in the studied galaxies for the (a) "instantaneous" star-formation mode (IB) and the (b) extended star-formation mode (EB).

it difficult to compare the colors, and a comparison of the color excesses of objects of different sizes and, consequently, different stellar compositions, is likewise not totally correct. However, since light is absorbed not only inside the SFCs, but also largely in their peripheries, the radiation from small objects included in larger complexes undergoes approximately the same absorption as the radiation of the entire SFC. For our standard uncertainty in the estimated interstellar absorptions 0.45^m, the standard uncertainty in the color excess is $\sigma_{E_{B-V}} = 0.14^m$. This is comparable with the observational accuracies of the color excesses obtained in [22], which range from 0.02^m to 0.26^m. A moderate, but appreciable correlation ($r = 70\%$) between the "model" and observed color excesses E_{B-V} (Fig. 7) appears to confirm the above suggestion.

The systematic excess of the interstellar absorption in gas emission lines, E^{gas}_{B-V}, over that in the stellar continuum, E^{stars}_{B-V}, is also confirmed. The slope of the linear dependence, ≈ 1.5, coincides with previously obtained relations between the "gas" (E^{gas}_{B-V}) and "stellar" (E^{stars}_{B-V}) absorptions [23–26].

Figure 8 presents the age distributions for the SFCs in the five galaxies for the two star-formation modes separately. For the IB mode in Fig. 8a, the SFCs are divided into two age groups. The basic group of objects has ages of 1–7 million years, while several SFCs form a second group with ages of 12–14 million years. Ages up to 7 million years and the gas velocities in a giant HII region, 15–30 km/s, correspond to sizes of about 100 pc, while ages up to 14 million years and a single "burst" of star formation in the SFC correspond to sizes of about 200 pc. This may indicate a discrepancy between the physical sizes of the SFCs and the size of the diaphragm in the Hα+ [NII] filter, and explain the absence of any correlation between these sizes and the brightnesses of the objects. The age distribution of the SFCs for the EB star-formation mode generally corresponds to the normal law $\overline{t} = 40 \pm 30$ million years (Fig. 8b). The deviation from a normal distribution in NGC 4656/57 is due to the small size of the sample, which contains only five objects.

All the studied galaxies display signs of star formation induced by activity in their nuclei or gravitational interaction. NGC 1068 is a compact spiral Sb Seyfert galaxy. The relatively large nuclear brightness and large width of the gas emission lines in the nuclear spectrum provide evidence for active energy-release processes there. NGC 4631 is a giant Sc spiral connected with the NGC 4656/57 system by a hydrogen bridge. NGC 4656 is an interacting Sc galaxy. The bright spot at the eastern edge of the galaxy is a region of intense star formation; it is considered to be a separate system with its own designation, NGC 4657. The interaction with the galaxy NGC 4631 results in a bend at the eastern end of the bright star-formation region of NGC 4657, intense star formation in NGC 4657, and the hydrogen bridge to NGC 4631. NGC 4490 is an Sc spiral galaxy interacting with the irregular galaxy NGC 4485. NGC 4449 is a dwarf irregular galaxy; whose star formation may be catalyzed by interaction with nearby galaxies.

A more complete study of the star-formation parameters in the studied SFCs may reveal a relation between the origins of induced star formation (nuclear activity or gravitational interaction) and the distributions of the star-formation parameters. This study requires spectral observations that can provide obtain independent measurements of the chemical compositions and interstellar absorptions. It is of interest to compare the latter with our estimates obtained using

Table 2. Parameters of the absorption distributions in SFCs in the studied galaxies

NGC	N	A_V^G	Type of distribution
1	2	3	4
1068	23	0.21^m	Normal, $\overline{A_V} = 1.1 \pm 0.6$
4449	18	0.15^m	$N = 0.5 + 13.4 \exp\left(-\dfrac{A_V - 0.375}{0.44}\right)$
4490	27	0.15^m	$N = -8.1 + 24.3 \exp\left(-\dfrac{A_V - 0.375}{2.17}\right)$
4631	38	0.14^m	$N = (18.9 \pm 0.8) - (4.5 \pm 1.2)A_V - (0.9 \pm 0.4)A_V^2$
4656/57	8	0.14^m	Normal, $\overline{A_V} = 0.9 \pm 0.4$

a grid of evolutionary models. Our further studies will be devoted to investigating these questions.

ACKNOWLEDGMENTS

This work was partially supported by the Russian Foundation for Basic Research (project codes 08-02-01323, 06-02-16379, and 07-02-00792) and a Presidential Grant of the Russian Federation for the Support of Young Russian Candidates of Science (MK-4818.2007.2). The authors thank V.A. Gagen-Thorn (University of St. Petersburg) for useful remarks.

REFERENCES

1. V. Myakutin, A. E. Piskunov, F. Sakhibov, and M. A. Smirnov, in *XXIInd General Assembly of the IAU, Astronomy Poster Abstracts,* Ed. by H. van Woerden (Twin Press, Sliedrecht, 1994), p. 59.
2. A. S. Gusev, V. I. Myakutin, F. Kh. Sakhibov, and M. A. Smirnov, Astron. Zh. **84**, 266 (2007) [Astron. Rep. **51**, 234 (2007)].
3. F. Kh. Sakhibov and M. A. Smirnov, Astron. Zh. **81**, 998 (2004) [Astron. Rep. **48**, 909 (2004)].
4. F. Kh. Sakhibov and M. A. Smirnov, Astron. Zh. **78**, 3 (2001) [Astron. Rep. **45**, 1 (2001)].
5. F. Sakhibov and M. A. Smirnov, Astron. Astrophys. **354**, 802 (2000).
6. J. M. Scalo, *The Stellar Initial Mass Function, Fundamentals of Cosmic Physics,* Vol. 11 (Texas Univ. Press, Austin, 1986).
7. F. Kh. Sakhibov and M. A. Smirnov, Astron. Zh. **76**, 419 (1999) [Astron. Rep. **43**, 361 (1999)].
8. A. E. Piskunov and V. I. Myakutin, Astron. Zh. **73**, 520 (1996) [Astron. Rep. **40**, 472 (1996)].
9. E. E. Salpeter, Astrophys. J. **121**, 161 (1955).
10. A. Zurita, M. Rozas, and J. E. Beckman, Astron. Astrophys. **363**, 9 (2000)
11. Yu. N. Efremov and B. Elmegreen, Mon. Not. R. Astron. Soc. **299**, 588 (1998).
12. I. I. Pronik and K. K. Chuvaev, Izv. Krym. Astrofiz. Obs. **38**, 219 (1967).
13. I. I. Pronik and K. K. Chuvaev, Izv. Krym. Astrofiz. Obs. **40**, 96 (1969).
14. I. I. Pronik and K. K. Chuvaev, Izv. Krym. Astrofiz. Obs. **43**, 101 (1971).
15. I. I. Pronik, Izv. Krym. Astrofiz. Obs. **45**, 162 (1972).
16. B. P. Artamonov, Izv. Spets. Astrofiz. Obs. **6**, 27 (1974).
17. S. A. Dobrodii and I. I. Pronik, Izv. Krym. Astrofiz. Obs. **60**, 66 (1979).
18. N. B. Grigor'eva, Izv. Krym. Astrofiz. Obs. **54**, 171 (1976).
19. N. B. Grigor'eva, Izv. Krym. Astrofiz. Obs. **59**, 194 (1979).
20. N. B. Grigor'eva, Izv. Krym. Astrofiz. Obs. **62**, 39 (1980).
21. H. L. Johnson, Ann. Rev. Astron. Astrophys. **4**, 193 (1966).
22. A. Smith, N. Collins, W. Waller, et al., Astrophys. J. **546**, 829 (2001).
23. J. Caplan and L. Deharveng, Astron. Astrophys. **155**, 297 (1986).
24. F. Kh. Sakhibov and M. A. Smirnov, Astron. Zh. **72**, 318 (1995) [Astron. Rep. **39**, 281 (1995)].
25. J. Maiz-Apellaniz, J. M. Mas-Hesse, C. Munoz-Tunon, and H. O. Castanede, Astron. Astrophys. **329**, 409 (1998).
26. R. Cid Fernandes, A. Mateus, L. Sodre, Jr., et al., Mon. Not. R. Astron. Soc. **358**, 363 (2005).

Translated by K. Maslennikov